Sensorless Field-Orientation Control of an Induction Machine by High-Frequency Signal Injection

Jung-Ik Ha, *Student Member, IEEE*, and Seung-Ki Sul, *Senior Member, IEEE*

***Abstract*— This paper describes a new scheme to find the rotor flux angle from stator voltages and currents by injecting high-frequency signal. The signal is not a rotating one, but a fluctuating one at a synchronous rotating reference frame with the fundamental stator frequency. When the estimated rotor flux angle coincides with the actual angle, the proposed method makes virtually no ripple torque, no vibration, and less audible noise caused by the injected signal. The difference of impedances between the flux axis and the quadrature axis at high-frequency signal injection on the rotor flux angle is explained by the equivalent circuit equation of the induction machine. The difference is verified by experiments on the test motors at various testing conditions. The sensorless field-orientation algorithm is proposed, and the experimental results clarify the satisfactory operation of the algorithm with 150% load torque at zero stator frequency.**

***Index Terms*— Field-orientation control, induction machine, sensorless control.**

I. Introduction

THE sensorless drive of an induction machine has been studied for last two decades, and some of the results are applied to industrial fields [1], [2]. However, the performance of the drive is still much inferior to that of the sensored drive. In particular, at low or zero stator frequency, the torque controllability of the drive is still far from satisfactory. At higher stator frequency, practically, higher than 10% of rated frequency, simple direct vector control method based on the integration of the stator terminal voltages gives satisfactory torque control performance [3]. Most of the sensorless drive algorithms are based on the assumption of d–q equivalent circuit of the induction machine [4]–[7] and, hence, they are dependent on the machine parameters and measurement errors. At low stator frequency region, signal-to-noise ratio of the stator voltage measurement is very poor and stator resistance voltage drop is dominant. At zero stator frequency, even theoretically no rotor dynamics can be measured at the stator terminals [8]. For these reasons, the sensorless algorithm based on d-q circuit fails at low and zero stator frequency region, no matter how superior is the algorithm. Another group of sensorless algorithms uses nonideal phenomenon of the machine characteristics, such as eccentricity of rotor, rotor slot harmonics, and rotor unbalance [9], [10]. These algorithms need frequency spectrum analysis, and they are time consuming and need some machine construction data, such as number of rotor and stator slot, which cannot be easily obtained off the shelf. Even with the newly developed fast Fourier transform (FFT) algorithm, the performance of the speed control bandwidth of the drive still looks unsatisfactory [11]. The third category of the algorithm injects some signals to the motor and checks the response of the motor to the injected signals [12]–[15]. Most of these algorithms depend on the variation of rotor leakage inductance according to the intensity of the main flux. This algorithm gives reasonably satisfactory performance for the open rotor slot motor, but, in the case of the closed rotor slot, which, unfortunately, is the case for most small- and medium-power squirrel-cage induction machines, the algorithm does not work well, in particular, at loaded operating condition, because of a similar saturation effect on the leakage inductance with load current flowing in the rotor circuit. The torque controllability at low and zero frequency region could be a great asset to an off-the-shelf general purpose inverter feeding a conventional squirrel-cage induction motor. So far, most algorithms do not work well with mass-produced closed rotor slot motors in zero or low stator frequency region under heavily loaded condition.

In this paper, a new algorithm based on harmonic signal injection to the motor is proposed. The method can be implemented on the existing digitally controlled inverter by only amending the software of the inverter, without any extra hardware. It injects a fluctuating signal to the motor on the estimated flux axis of the motor and the difference of the impedance of the motor between flux axis and quadrature axis is measured. Normally, the difference is not measurable at fundamental frequency, but is measurable at injected high frequency due to the skin effect. After some signal processing, field-orientation control is achieved with the difference of the impedance. This algorithm gives reasonable torque control capability at zero and low stator frequency, even under heavily loaded condition. As compared to another signal injection method [12], it injects not rotating signal, but fluctuating signal on the flux axis and, hence, it generates no torque ripple, no vibration, and less audible noise. Its signal processing is quite simple compared to the method in [13], where the Kalman filter approach is needed.

Paper IPCSD 98–54, presented at the 1997 Industry Applications Society Annual Meeting, New Orleans, LA, October 5–9, and approved for publication in the IEEE TRANSACTIONS ON INDUSTRY APPLICATIONS by the Industrial Drives Committee of the IEEE Industry Applications Society. Manuscript released for publication July 27, 1998.

The authors are with the School of Electrical Engineering, Seoul National University, Seoul, 151-742 Korea.

Publisher Item Identifier S 0093-9994(99)00466-1.

II. Impedance Difference on the d–q Axes at the High Frequency

The rotating high-frequency stator currents are governed predominantly by the stator and rotor leakage inductance. Therefore, if there is no spatial modulation in the rotor leakage inductance, no information about rotor position or flux angle can be detectable [8]. However, at zero or low speed, the effect on the fluctuating signals in the synchronously rotating reference frame differs from the effect on the rotating ones. Thus, it is possible to detect the information about rotor flux angle without any spatial modulation.

The well-known voltage equations for an induction machine are expressed as follows:

$$\begin{aligned} V_{ds}^e &= r_s i_{ds}^e + \frac{d\lambda_{ds}^e}{dt} - \omega_e \lambda_{qs}^e \\ V_{qs}^e &= r_s i_{qs}^e + \frac{d\lambda_{qs}^e}{dt} + \omega_e \lambda_{ds}^e \end{aligned} \tag{1}$$

$$\begin{aligned} 0 &= r_r i_{dr}^e + \frac{d\lambda_{dr}^e}{dt} - (\omega_e - \omega_r)\lambda_{qr}^e \\ 0 &= r_r i_{qr}^e + \frac{d\lambda_{qr}^e}{dt} + (\omega_e - \omega_r)\lambda_{dr}^e \end{aligned} \tag{2}$$

$$\begin{aligned} \lambda_{ds}^e &= L_s i_{ds}^e + L_m i_{dr}^e \\ \lambda_{qs}^e &= L_s i_{qs}^e + L_m i_{qr}^e \end{aligned} \tag{3}$$

$$\begin{aligned} \lambda_{dr}^e &= L_m i_{ds}^e + L_r i_{dr}^e \\ \lambda_{qr}^e &= L_m i_{qs}^e + L_r i_{qr}^e. \end{aligned} \tag{4}$$

By assuming the rotor-flux-oriented control, that is, $\lambda_{qr}^e = 0$, the stator currents are as follows:

$$\begin{aligned} i_{ds}^e &= -\frac{r_r + pL_r}{pL_m} i_{dr}^e \\ i_{qs}^e &= -\frac{L_r}{L_m} i_{qr}^e \end{aligned} \tag{5}$$

where p is a differntial operator. Then,

$$\begin{aligned} V_{ds}^e &= \left(r_s + p\sigma L_s + p\frac{r_r L_m^2}{L_r(r_r + pL_r)} \right) i_{ds}^e - \omega_e \lambda_{qs}^e \\ V_{qs}^e &= (r_s + p\sigma L_s) i_{qs}^e + \omega_e \lambda_{ds}^e. \end{aligned} \tag{6}$$

At zero or low stator frequency, where the magnitude of ω_e is quite small, if the high-frequency fluctuating signals are injected, $\omega_e \lambda_{qs}^e (\ll V_{ds}^e)$ and $\omega_e \lambda_{ds}^e (\ll V_{qs}^e)$ terms in (6) can be neglected. So, (6) can be rewritten as

$$\begin{aligned} V_{ds}^e &\approx \left(r_s + p\sigma L_s + p\frac{r_r L_m^2}{L_r(r_r + pL_r)} \right) i_{ds}^e \\ V_{qs}^e &\approx (r_s + p\sigma L_s) i_{qs}^e. \end{aligned} \tag{7}$$

In particular, for the high-frequency component, (7) can be rewritten as

$$\begin{aligned} \tilde{\nu}_{ds}^e &\approx \left(r_s + j\omega_h \sigma L_s + j\omega_h \frac{r_r L_m^2}{L_r(r_r + j\omega_h L_r)} \right) \tilde{i}_{ds}^e \\ \tilde{\nu}_{qs}^e &\approx (r_s + j\omega_h \sigma L_s) \tilde{i}_{qs}^e \end{aligned} \tag{8}$$

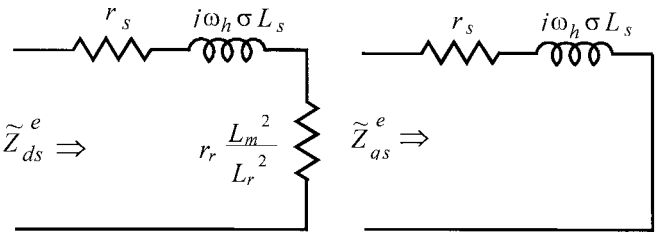

Fig. 1. Terminal impedances in the synchronous reference frame.

where

$$\begin{aligned} V_{ds}^e &= V_{ds1}^e + \tilde{\nu}_{ds}^e = V_{ds1}^e + V_{ds}^e \sin(\omega_h t) \\ V_{qs}^e &= V_{qs1}^e + \tilde{\nu}_{qs}^e = V_{qs1}^e + V_{qs}^e \sin(\omega_h t + \phi). \end{aligned}$$

"$\sim$" is the operator meaning the high-frequency component in the steady state.

Generally, because the rotor resistor r_r is much smaller than $\omega_h L_r$, it can be assumed that $r_r + j\omega_h L_r \approx j\omega_h L_r$. Then, (8) is expressed as (9). The d–q equivalent circuits at the injected high frequency can be shown as in Fig. 1

$$\begin{aligned} \tilde{\nu}_{ds}^e &\approx \left(r_s + r_r \frac{L_m^2}{L_r^2} + j\omega_h \sigma L_s \right) \tilde{i}_{ds}^e \equiv \tilde{Z}_d \tilde{i}_{ds}^e \\ \tilde{\nu}_{qs}^e &\approx (r_s + j\omega_h \sigma L_s) \tilde{i}_{qs}^e \equiv \tilde{Z}_q \tilde{i}_{qs}^e. \end{aligned} \tag{9}$$

Due to the skin effect at high frequency, the value of rotor resistor r_r is dozens of times as large as that at fundamental frequency and, by the skin effect, the value of σL_s becomes much smaller at high frequency than that at fundamental frequency [16]. Thus, because the contribution of rotor resistance term to the terminal impedance (Z_d) is increased relative to the reactance term, it is apparent that the difference between the d- and q-axes terminal impedance is detectable

$$\tilde{Z}_d > \tilde{Z}_q. \tag{10}$$

Hence, for the fluctuating signals in the synchronously rotating reference frame, the impedance measured on the rotor flux axis differs from that on the quadrature axis to the rotor flux. The fluctuating signals result in eddy-current loss, additional copper loss, hysteresis loss, stray loss, and so on. So, the level of injected signal should be kept as small as possible.

III. Control Strategy

A. Measurement for Flux Angle Tracking

For tracking of flux angle, the high-frequency fluctuating signal on the estimated d axis in the synchronous reference frame is used. At starting, an arbitrary axis is preassumed as the estimated axis. The effect of the signal can be measured into the orthogonal measurement axes, the d_m^e and q_m^e axes as shown in Fig. 2. If the estimated d axis is between the flux

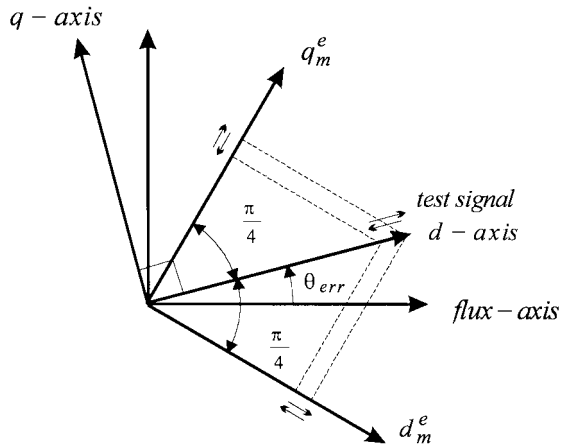

Fig. 2. Test axis and measure axis in the synchronous reference frame.

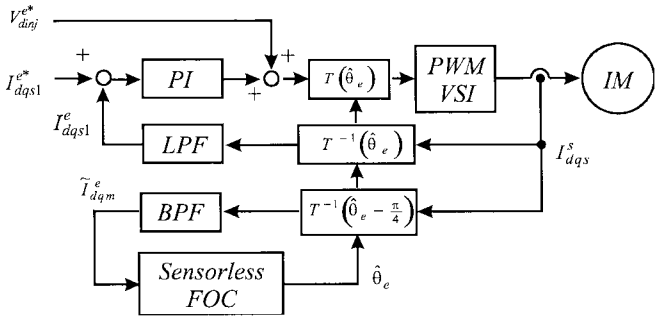

(a)

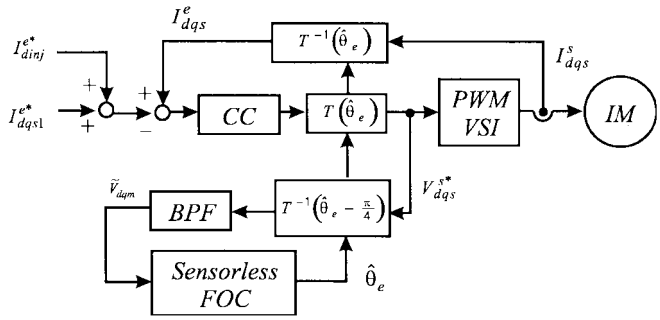

(b)

Fig. 3. Proposed sensorless field-orientation schemes using high-frequency signal injection. (a) High-frequency voltage injection scheme. (b) High-frequency current injection scheme.

axis and quadrature axis, then the measured high-frequency components on the d_m^e and q_m^e axes would be different.

B. High-Frequency Signal Injection

In the implementation of the measurement of the injected signals, there are the voltage injection method and the current injection method. The injecting signal in the former is added to the d-axis component of the current controller output, as shown in Fig. 3(a). In this method, for the purpose of avoiding the cancellation of the injected signal by the current controller, the

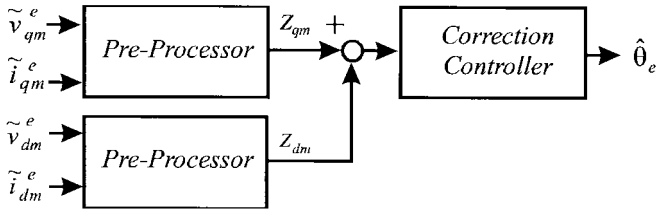

Fig. 4. Proposed sensorless field-orientation controller using high-frequency signals measured on the d_m^e and q_m^e axes.

bandwidth of the current controller should be let down and the filtered signals should be used in the feedback control. In the latter, the injecting signal is added to the fundamental current reference on the d axis, as shown in Fig. 3(b). In order to inject high-frequency current correctly, the current controller should have sufficient bandwidth. The former has the inherent limitation of current control and speed control bandwidth, but the signals are less vulnerable to nonlinear effect such as dead-time effect. The latter has the possibility of higher bandwidth of speed control, but it requires more elegant signal processing against the nonlinear effects of the system.

C. Field-Orientation Scheme

The signals measured on the d_m^e and q_m^e axes are used in tracking of the rotor flux angle, as shown in Fig. 4. In the preprocess, the information correlated to the impedance at the injected high frequency is calculated on the d_m^e and q_m^e axes. In the correction controller, using these impedances obtained in the preprocess, the tracking of the flux angle is carried out.

In the high-frequency voltage injection method, if the injected voltage is fixed, the terminal impedances on the measurement axes depend on the measured currents. The difference between the square of $|\tilde{i}_{dm}^e|$ and that of $|\tilde{i}_{qm}^e|$ is proportional to the difference of the admittances measured on the each axis. In the high-frequency current injection method, there are similar relations. Therefore, the schemes in Fig. 3. are plausible in each case.

Relations between terminal voltages and currents on the measurement axes are expressed in

$$\tilde{\nu}_{dm}^e \approx \left(r_s + \frac{r_r L_m^2}{2L_r^2}\left[1+\cos\left(2\theta_{\rm err}-\frac{\pi}{2}\right)\right] + j\omega_h \sigma L_s\right)\tilde{i}_{dm}^e$$
$$\tilde{\nu}_{qm}^e \approx \left(r_s + \frac{r_r L_m^2}{2L_r^2}\left[1+\cos\left(2\theta_{\rm err}+\frac{\pi}{2}\right)\right] + j\omega_h \sigma L_s\right)\tilde{i}_{qm}^e \tag{11}$$

where

$\theta_{\rm err} = \hat{\theta}_e - \theta_e$;
θ_e actual rotor flux angle;
$\hat{\theta}_e$ estimated rotor flux angle.

Case 1—High-Frequency Voltage Injection:

$$\text{Injected voltages} \quad \tilde{\nu}_{dm}^e = \tilde{\nu}_{qm}^e = \frac{V_{\rm inj}^*}{\sqrt{2}}\sin(\omega_h t). \tag{12}$$

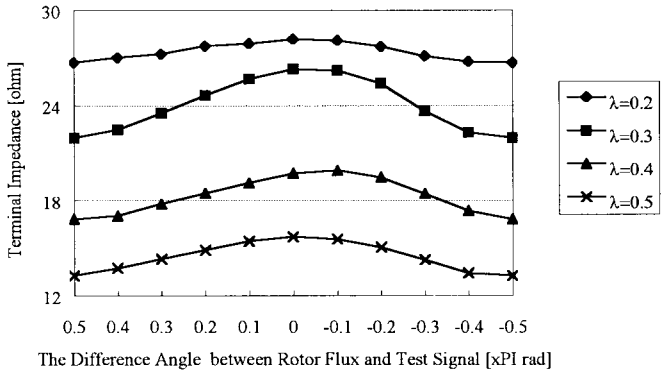

Fig. 5. Impedance at various flux levels (5-hp induction machine, unit of λ: Wb, test signal: 500 Hz).

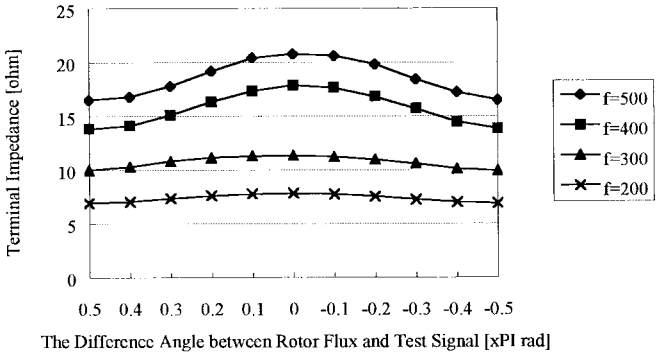

Fig. 6. Impedance at various frequencies (5-hp induction machine, unit of f: Hz, at rated flux).

Error of measured signals

$$\begin{aligned}\text{Err} &\equiv \left|\tilde{i}^e_{dm}\right|^2 - \left|\tilde{i}^e_{qm}\right|^2 \\ &\approx -\frac{V^{*2}_{\text{inj}} r_r \frac{L_m^2}{L_r^2}\left(r_s + r_r \frac{L_m^2}{2L_r^2}\right)\sin 2\theta_{\text{err}}}{\left|\left(r_s + j\omega_h \sigma L_s + r_r \frac{L_m^2}{L_r^2}\right)\left(r_s + j\omega_h \sigma L_s\right)\right|^2} \\ &\approx \frac{V^{*2}_{\text{inj}} r_r \frac{L_m^2}{L_r^2}\left(2r_s + r_r \frac{L_m^2}{L_r^2}\right)}{\left|\left(r_s + j\omega_h \sigma L_s + r_r \frac{L_m^2}{L_r^2}\right)\left(r_s + j\omega_h \sigma L_s\right)\right|^2}(\theta_e - \hat{\theta}_e) \\ &\equiv Y_{\text{err}}(\theta_e - \hat{\theta}_e). \end{aligned} \tag{13}$$

Frequency response function relating the estimated and actual rotor angles

$$\frac{\hat{\theta}_e(s)}{\theta_e(s)} = \frac{K_1 s + K_2}{s^2 + K_1 s + K_2} \tag{14}$$

where the controller

$$G(s) = \frac{1}{s}\left(K_P + \frac{K_I}{s}\right)$$

$$K_1 = Y_{\text{err}} K_P, \quad K_2 = Y_{\text{err}} K_I.$$

Case 2—High-Frequency Current Injection:

$$\text{Injected currents} \quad \tilde{i}^e_{dm} = \tilde{i}^e_{qm} = \frac{I^*_{\text{inj}}}{\sqrt{2}}\sin(\omega_h t). \tag{15}$$

Error of measured signals

$$\begin{aligned}\text{Err} &\equiv \left|\tilde{\nu}_{qm}\right|^2 - \left|\tilde{\nu}_{dm}\right|^2 \\ &= -I^{*2}_{\text{inj}} r_r \frac{L_m^2}{2L_r^2}\left(2r_s + r_r \frac{L_m^2}{L_r^2}\right)\sin 2\theta_{\text{err}} \\ &\approx I^{*2}_{\text{inj}} r_r \frac{L_m^2}{L_r^2}\left(2r_s + r_r \frac{L_m^2}{L_r^2}\right)(\theta_e - \hat{\theta}_e) \\ &\equiv Z_{\text{err}}(\theta_e - \hat{\theta}_e). \end{aligned} \tag{16}$$

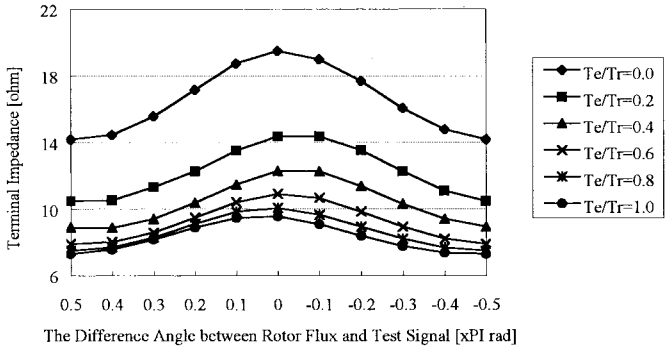

Fig. 7. Impedance under various load torque (5-hp induction machine, Te, Tr: output torque and rated torque, at rated flux, test signal: 500 Hz).

Frequency response function relating the estimated and actual rotor angles

$$\frac{\hat{\theta}_e(s)}{\theta_e(s)} = \frac{K_1 s + K_2}{s^2 + K_1 s + K_2} \tag{17}$$

where the controller

$$G(s) = \frac{1}{s}\left(K_P + \frac{K_I}{s}\right)$$

$$K_1 = Z_{\text{err}} K_P, \quad K_2 = Z_{\text{err}} K_I.$$

The error is in the form of a linear angle error, such as (13) and (16). This error can be driven away using the scheme as shown in Fig. 4.

IV. Experimental Results

A. Measurement of High-Frequency Impedance Difference

At the high frequency, the difference of terminal impedance in the excited induction machine is examined in a test motor and shown in Figs. 5–8. A 5-hp general purpose induction machine is used in the experiments, and its characteristics

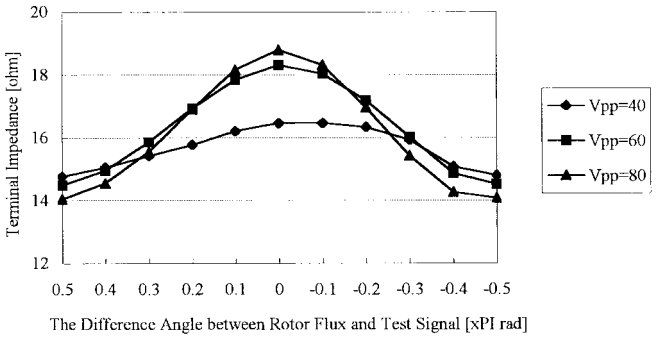

Fig. 8. Impedance at various injected voltages (5-hp induction machine, unit of $V_{\rm pp}$: V, test signal: 500 Hz, at rated flux).

TABLE I
TEST INDUCTION MACHINE

Rated Power	5 hp
Rated Voltage	220/440V
Number of Phase	3
Number of Pole	4
Rated Frequency	60 Hz
Rated Speed	1730 rpm
Frame	112M
Type of Rotor and Rotor Slot	squirrel cage closed slot

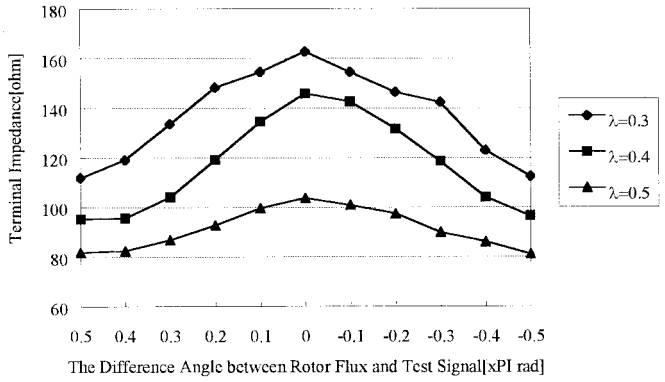

Fig. 9. Impedance at various flux levels (1-hp induction machine, unit of λ: Wb, test signal: 500 Hz).

are listed in Table I. The impedance on the rotor flux axis is higher than that on any other axis. Similar aspects appeared in the different power rating general purpose induction machines. Figs. 9 and 10 are test results for 1-hp and 10-hp induction machines with closed rotor slots, respectively.

The spatial difference of the terminal impedances in various conditions with the 5-hp machine is measured. They are measured using the fluctuating signals in the synchronous reference frame. The higher frequency of the injected signal makes for a great difference of impedances, as shown in Fig. 6. In Fig. 7, the difference of impedances is shown at various

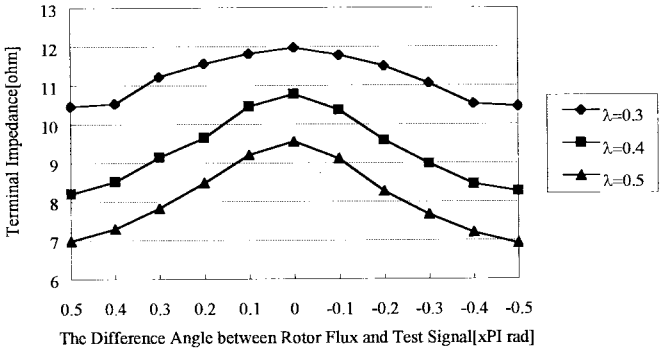

Fig. 10. Impedance at various flux levels (10-hp induction machine, unit of λ: Wb, test signal: 500 Hz).

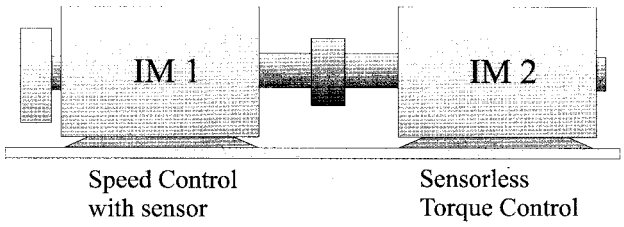

Fig. 11. System configuration for the experiments of sensorless field-orientation control.

load conditions. This result is performed under locked rotor. As the intensity of the injected signal is getting stronger, the difference is larger, as shown in Fig. 8. Through the above experimental results, the impedance at rotor flux axis is larger than that on any other axis is confirmed.

B. Field-Orientation Control

Fig. 11 shows the system configuration for the experiments of the proposed sensorless field-orientation control. For the experiments at zero and low stator frequency, the induction machine 1 is running in the speed control mode with the sensored field-orientation control, and the induction machine 2, which is under test, is in the torque control mode with the proposed sensorless control. Digitally controlled voltage-fed pulsewidth modulation insulated gate bipolar transistor (PWM IGBT) inverters are used for this experiment, and their main processor is a TMS320C31.

The experimental results under 75% and 150% step load are shown in Figs. 12 and 13, respectively. The measured rotor speed, the flux angle calculated using rotor speed and stator current, the estimated rotor flux position, and the estimated torque and phase currents are illustrated in each figure. In the experiments, the torque is estimated in motor 1. Hence, the generated torque by motor 2 has the reverse sign of the estimated torque. When the system is under the load, the stator frequency of motor 2 is zero.

At no load condition, the flux angle coincides with current angle. Therefore, the injected signals appear near the peak of phase current. However, under load condition, the torque current is higher than the flux current. In this case, the higher

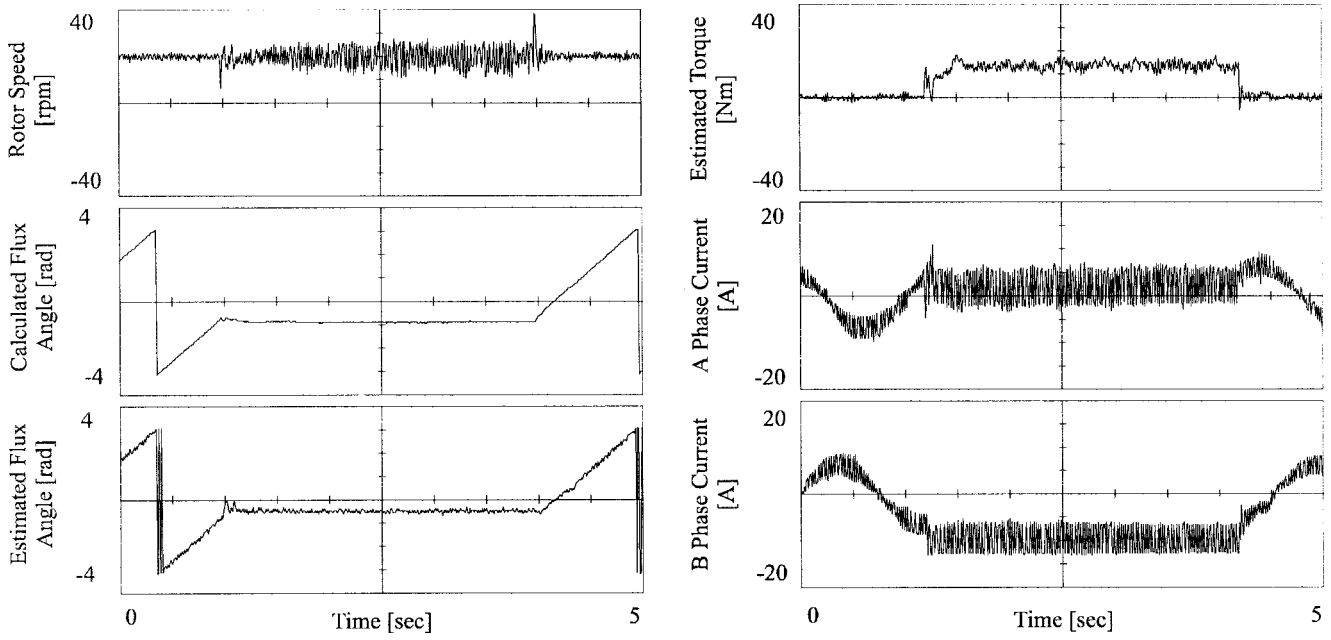

Fig. 12. Step torque response of the proposed system under 75% step load.

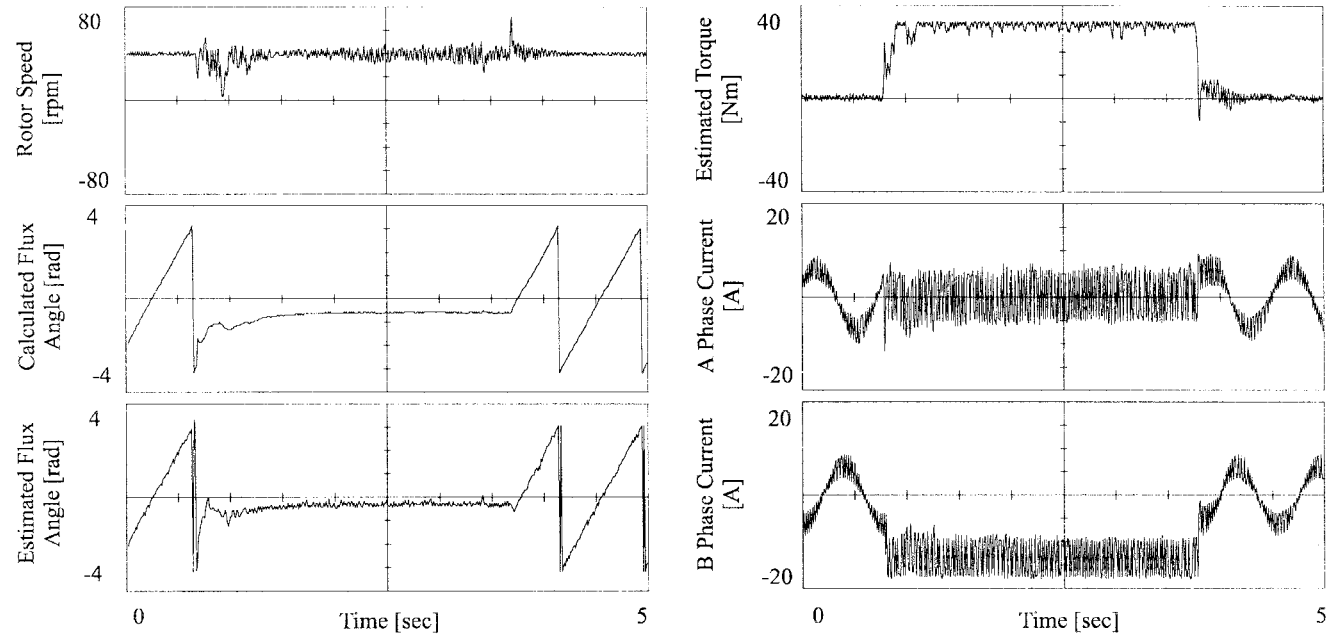

Fig. 13. Step torque response of the proposed system under 150% step load.

injected signals appear near the lower level of phase current shown in Figs. 12 and 13. From Fig. 12, it can be seen that the speed of the machines is maintained at 20 r/min, regardless of load torque variation due to the speed control of motor 1, and that the torque of motor that is under test is following its command. The stator frequency of motor 2 is changing from 2/3 Hz to 0 Hz and back to 2/3 Hz according to the torque. In Fig. 13, the same test is done with 150% rated load torque command. The traces of Figs. 12 and 13 show clearly that motor 2 is under torque servo mode, even at zero stator frequency. In Fig. 14, the traces of stator currents with injected high frequency at 75% torque are shown, where the quadrature axis to the flux axis coincides with the B phase of the motor.

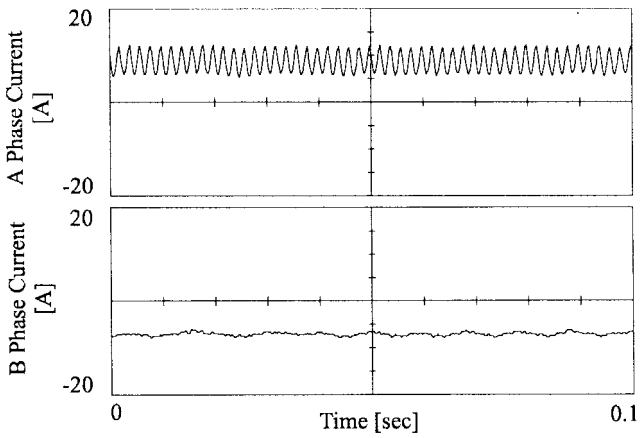

Fig. 14. Stator currents in high-frequency signal injection at zero stator frequency under 75% rated load torque.

V. Conclusion

The difference of the terminal impedances in the synchronously rotating reference frame by fluctuating high-frequency signal is brought out. The difference is explained by induction motor equivalent equation and measured in test machines. The control scheme for sensorless field orientation using this difference has been proposed and verified by the experimental results. This method has stable steady-state performance and transient dynamics at zero or low stator frequency by injected voltage or current information. It is not influenced by machine parameters in the accuracy of sensorless flux angle estimation with general purpose off-the-shelf squirrel-cage induction machine.

References

[1] T. Ohtani, N. Takada, and K. Tanaka, "Vector control of an induction motor without shaft encoder," *IEEE Trans. Ind. Applicat.*, vol. 28, pp. 157–164, Jan./Feb. 1992.

[2] M. Depenbrock, "Direct self-control (DSC) of inverter-fed induction machine," *IEEE Trans. Power Electron.*, vol. 3, pp. 420–429, Oct. 1988.

[3] K. D. Hurst, T. G. Habetler, G. Griva, and F. Profumo, "Zero-speed tacho-less I.M. torque control: Simply a matter of stator voltage integration," in *Conf. Rec. IEEE APEC'97*, 1997, pp. 749–753.

[4] C. Schauder, "Adaptive speed identification for vector control of induction motors without rotational transducers," in *Conf. Rec. IEEE-IAS Annu. Meeting*, 1989, pp. 493–499.

[5] Tajima and Y. Hori, "Speed sensorless field orientation control of the induction machine," in *Conf. Rec. IEEE-IAS Annu. Meeting*, 1991, pp. 385–391.

[6] R. Kim, S. K. Sul, and M. H. Park, "Speed sensorless vector control of an induction motor using an extended Kalman filter," in *Conf. Rec. IEEE-IAS Annu. Meeting*, 1992, pp. 594–599.

[7] H. Kubota and K. Matsuse, "Speed sensorless field oriented control of induction machines," *IEEE Trans. Ind. Applicat.*, vol. 30, pp. 1219–1224, Sept./Oct. 1994.

[8] J. Holtz, "Speed estimation and sensorless control of AC machine," in *Conf. Rec. IEEE IECON'93*, 1993, pp. 649–661.

[9] M. Ishida and K. Iwata, "A new slip frequency detector of an induction motor utilizing motor slot harmonics," *IEEE Trans. Ind. Applicat.*, vol. IA-20, pp. 575–582, May/June 1984.

[10] K. D. Hurst and T. G. Habetler, "Sensorless speed measurement using current harmonics spectral estimation in induction machine drives," *IEEE Trans. Power Electron.*, vol. 11, pp. 66–73, Jan. 1996.

[11] A. Ferrah, K. J. Bradley, P. J. Hogben, M. S. Woolfson, and G. M. Asher, "A transputer-based speed identifier for induction motor drives using real-time adaptive filtering," in *Conf. Rec. IEEE-IAS Annu. Meeting*, 1997, pp. 394–400.

[12] P. L. Jansen and R. D. Lorenz, "Transducerless field orientation concepts employing saturation-induced saliencies in induction machines," in *Conf. Rec. IEEE-IAS Annu. Meeting*, 1995, pp. 174–181.

[13] M. Schroedl, "Sensorless control of AC machines at low speed and standstill based on the "INFORM" method," in *Conf. Rec. IEEE-IAS Annu. Meeting*, 1996, pp. 270–277.

[14] F. Blaschke, T. van der Burgt, and A. Vandenput, "Sensorless direct field orientation at zero flux frequency," in *Conf. Rec. IEEE-IAS Annu. Meeting*, 1996, pp. 189–196.

[15] S. I. Yong, J. W. Choi, and S. K. Sul, "Sensorless vector control of induction machine using high frequency current injection," in *Conf. Rec. IEEE-IAS Annu. Meeting*, 1994, pp. 503–508.

[16] T. Yokozuka, E. Baba, and T. Takatsuki, "Input impedance and losses of induction motors operating from inverters," *Trans. Inst. Elect. Eng. Jpn.*, vol. 117-D, no. 10, pp. 1254–1261, 1997.

Jung-Ik Ha (S'97) was born in Pusan, Korea, in 1971. He received the B.S. and M.S. degrees in electrical engineering in 1995 and 1997, respectively, from Seoul National University, Seoul, Korea, where he is currently working towards the Ph.D. degree.

His research interests are electric machine drives and electric propulsion systems.

Seung-Ki Sul (S'78–M'80–SM'98) was born in Korea in 1958. He received the B.S., M.S., and Ph.D. degrees in electrical engineering from Seoul National University, Seoul, Korea, in 1980, 1983, and 1986, respectively.

He was an Associate Researcher with the Department of Electrical and Computer Engineering, University of Wisconsin, Madison, from 1986 to 1988. From 1988 to 1990, he was a Principal Research Engineer with Gold-Star Industrial Systems Company. Since 1991, he has been with the School of Electrical Engineering, Seoul National University, where he is currently an Associate Professor. His current research interests are power electronics control of electric machines, electric vehicle drives, and power converter circuits.